

Searching for high magnetization density in bulk Fe: the new metastable Fe₆ phase

Koichiro Umemoto,^{1,2} Burak Himmetoglu,³ Jian-Ping Wang,⁴ Renata M. Wentzcovitch,⁵ and Matteo Cococcioni^{*5}

¹*Department of Earth Sciences, University of Minnesota, Minneapolis, MN 55455, USA*

²*Earth-Life Science Institute, Tokyo Institute of Technology,
2-12-1-IE-1 O Okayama, Meguro-ku, Tokyo, 152-8550, Japan*

³*Materials Department, University of California, Santa Barbara, CA 93106, USA*

⁴*Department of Electrical and Computer Engineering,
University of Minnesota, Minneapolis, MN 55455, USA*

⁵*Department of Chemical Engineering and Materials Science,
University of Minnesota, Minneapolis, Minnesota 55455, USA*

(Dated: March 27, 2021)

We report the discovery of a new allotrope of iron by first principles calculations. This phase has *Pmn*2₁ symmetry, a six-atom unit cell (hence the name Fe₆), and the highest magnetization density (M_s) among all known crystalline phases of iron. Obtained from the structural optimizations of the Fe₃C-cementite crystal upon carbon removal, *Pmn*2₁ Fe₆ is shown to result from the stabilization of a ferromagnetic FCC phase, further strained along the Bain path. Although metastable from 0 to 50 GPa, the new phase is more stable, at low pressures, than the other well-known HCP and FCC allotropes and smoothly transforms into the FCC phase under compression. If stabilized to room temperature, e.g., by interstitial impurities, Fe₆ could become the basis material for high M_s rare-earth-free permanent magnets and high-impact applications such as, light-weight electric engine rotors or high-density recording media. The new phase could also be key to explain the enigmatic high M_s of Fe₁₆N₂, which is currently attracting an intense research activity.

PACS numbers:

Permanent magnets are at the core of applications of unquestionable technological relevance. A high magnetization density (M_s) is certainly a very desirable feature in these systems as it would help the miniaturization of magnetic devices (e.g., for high storage density memories) and allow for lighter, more cost-effective applications. Most of currently available permanent magnets are rare-earth (RE) compounds. The extreme scarcity of these elements and their uneven distribution have stimulated, in the last decades, a vigorous search for magnetic materials based on earth-abundant elements [1–3], sometimes with a strong focus on nano-structured materials [4, 5]. Transition metals (TM) are the natural best alternative to RE for fabricating magnetic devices. On the other hand, *p*-type magnetism seems less promising for the above-mentioned applications. Although elements with open *p* shells are, in fact, very abundant, and tend to form light-weight compounds, the magnetization of these materials is often due to impurities and other kinds of point defects which implies that the resulting magnetic moments are highly diluted and lead to lower values of M_s . [6–8]. TM-based materials offer, in this sense, better opportunities to fabricate permanent magnets: due to their marked atomic character and scarce hybridization, *d* shells remain partially filled (open) more frequently than *p* shells and their higher degree of localization makes Hund’s exchange interaction stronger than for *p* states. For high M_s applications, *3d* TM elements are obviously

most appealing. While permanent magnetism is possible in their compounds (in fact, it was discovered in Fe₃O₄ magnetite) the presence of other, non-magnetic elements obviously decreases their volume-specific magnetization. In contrast, bulk elemental transition metals are usually soft magnets. Furthermore, the partially itinerant character of their *d* electrons undermines Hund’s magnetic interactions and contributes to suppress their bulk magnetization. Nevertheless, there has been a considerable effort to stabilize useful magnetic phases of transition metals through alloying (e.g., Fe - Ni and Fe - Co compounds) or through doping.

Within the latter scenario, Fe nitrides have attracted great interest [9–13]. One of the most intriguing Fe-N compounds, Fe₁₆N₂, has been the object of a sixty years-long debate about the magnetization of its α'' ordered phase. The commonly accepted unit cell of this material is a tetragonally distorted 2x2x2 supercell of bcc iron with nitrogen impurities occupying one fourth of the octahedral interstitial sites. After the crystal structure of this phase was resolved from studying tempered N-doped martensites [14], most of the research on this material focused on the deposition of high M_s thin films, mostly through sputtering. A long controversy ignited on the magnetic properties of these films. Some groups reported evidence of a saturation magnetization (between 2.4 and 3.2 T) higher than that of α Fe (2.3 T) and exceeding the prediction of the Slater-Pauling theory [15–18]. Others failed to observe any deviation from the trend established by this theory based on itinerant magnetism [19–21], also obeyed by other Fe nitrides [22–26]. Recently, the interest on this material was re-sparked, by research in J.-P. Wang’s group. This group was able to deposit a

^{*}present address: Institute of Materials, École Polytechnique Fédérale de Lausanne (EPFL), CH-1015 Lausanne, Switzerland

thin film of Fe nitride with a Fe-N stoichiometry close to 8:1 that, after proper annealing, reproducibly showed a magnetization density exceeding 2.68 T [10, 27–29].

All ab-initio calculations performed in the last decade on this material, based on the crystal structure proposed by Jack [14], and have failed to find higher M_s than bulk Fe, even when using corrections to the DFT functionals (as DFT+U, or hybrid functionals) able to improve the description of electronic localization on d states [30–37]. The only exception remains the model proposed by Wang’s group [38], based on the existence of Fe_6N supermagnetic clusters with additional Fe atoms in their interstitials.

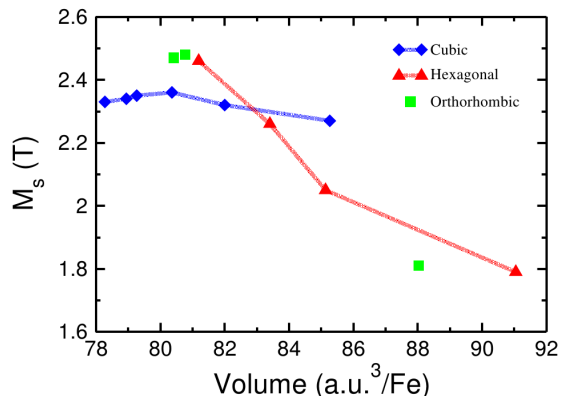


FIG. 1: (Color online) Magnetization density (in Tesla) of several Fe-N compounds at zero pressure. Lines are a guide to the eye. From left to right blue diamonds represent, bcc Fe, Fe_{64}N , Fe_{54}N , Fe_{32}N , Fe_{16}N , and Fe_{16}N_2 . Red triangles represent hcp Fe, Fe_{12}N , Fe_6N , Fe_3N . The green squares are relative to orthorhombic crystals and represent $Pmn2_1$ Fe_6 , $Pmmn$ Fe_6 , and $Pnma$ Fe_3N cementite (see text).

The present work is motivated by the controversial magnetic properties of this system. However, in this paper we deviate from the common approach of other works in literature and question the ability of the tetragonal α'' of Fe_{16}N_2 to express a high magnetization density. While Wang’s experiments [10, 27–29] suggest that the ordering of nitrogen impurities (achieved through annealing) probably plays a key role in determining the magnetic properties of the obtained crystal, the rich variety of Fe-N stoichiometries and the abundance of alternative crystalline phases open other possibilities that are worth considering. The idea we started exploring with the present paper is to obtain a crystal with the 16:2 stoichiometry from superstructures of other suitable Fe nitrides, whose nitrogen concentration is then properly adjusted. Following this line, we discovered a new (metastable) allotrope of iron, which shows the highest M_s of all known phases. This new crystal of iron could represent a first step towards the rationalization of the high M_s of the α'' phase of Fe_{16}N_2 and is the main focus of the present paper.

Results presented here are based on density-functional-theory (DFT) [39, 40]. The technical details of these calculations are briefly summarized in the footnote [56].

Our investigation started from a preliminary screening of the saturation magnetization density of different Fe nitrides, whose results are shown in Fig. 1. Based on the possibility of reaching higher values of M_s within the ϵ - Fe_3N family of compounds (red line), this stoichiometry was adopted as the starting point. However, due to the scarce resemblance with the tetragonal structure of the α'' phase, the hexagonal Fe_3N was disregarded. On the other hand, the tendency of C-doped Fe to form, upon slow cooling from the γ fcc solid solution, an orthorhombic crystal with the same C content (Fe_3C cementite) suggested the use of this structure as a starting point. Fe_3C cementite has a unit cell containing four formula units (shown in Fig. 2(a)) and a $Pnma$ space group. Its structure and symmetry are preserved when carbon is replaced by nitrogen, which results in a marginal volume increase. Although the unit cell of the cementite structure (Fe_{12}N_4) is not easily matchable with the 8:1 stoichiometry, it was used to qualitatively study the effect of nitrogen removal on the magnetic and structural properties of the crystal. In $Pnma$ Fe_3N nitrogen atoms

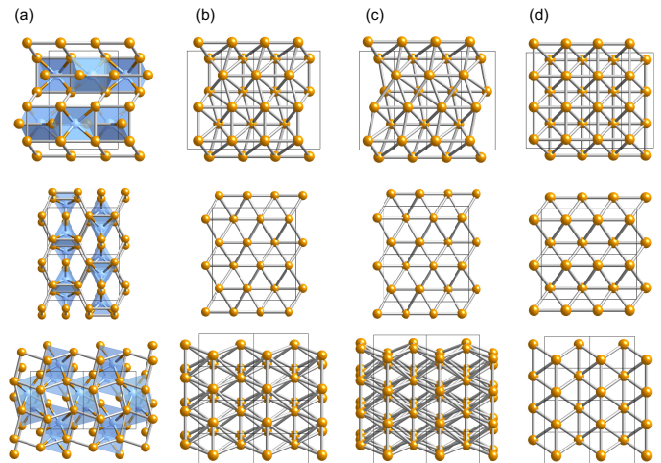


FIG. 2: Crystal structures of (a) cementite Fe_3N , (b) $Pmmn$ Fe_6 , (c) $Pmn2_1$ Fe_6 at 0 GPa and (d) $Pmn2_1$ Fe_6 at 70 GPa which is identical to fcc Fe. Orange and blue spheres denote iron and nitrogen, respectively. Upper, middle and lower rows correspond to the [001], [100], and [010] views of the Cementite crystal in column (a), to the [010], [001], and [100] views of the $Pmmn$ Fe_6 crystal in column (b), and to the [100], [010], and [001] views of the $Pmn2_1$ Fe_6 crystals in column (c) and (d).

occupy the center of trigonal prisms of irons, and are six-fold coordinated. The magnetic moment (per atom) and magnetization density of Fe_3N are relatively low: $2.05 \mu_B/\text{Fe}$ and 1.81 T, respectively. The removal of one nitrogen per cell does not affect significantly the structure of the crystal. Instead, when two or more nitrogen atoms are subsequently removed from the unit cell, giving Fe_6N , Fe_{12}N and pure Fe, respectively, structural optimization

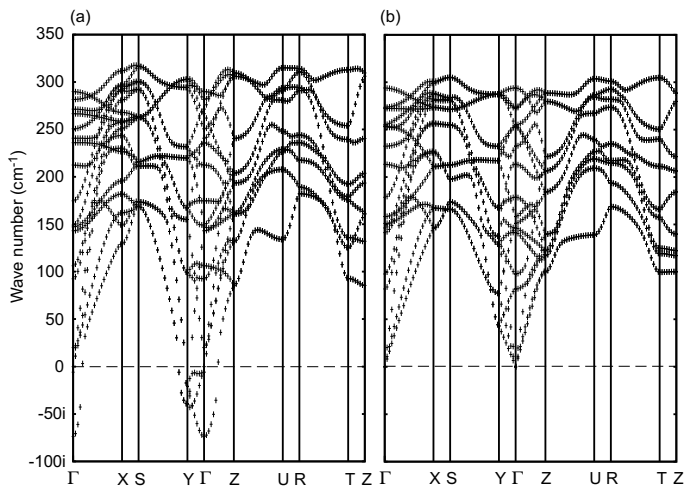


FIG. 3: Phonon dispersions at 0 GPa of (a) interim $Pmmn$ Fe_6 and (b) $Pmn2_1$ Fe_6 .

leads to a drastic change of the crystal structure. We focused our attention on the pure iron phase which assumes $Pmmn$ symmetry. The $Pmmn$ crystal structure, obtained upon extraction of all nitrogens from $Pnma$ -type Fe_3N , is shown in Fig. 2(b). Due to a translational symmetry, not present in the original $Pnma$ crystal, the unit cell of the $Pmmn$ Fe is half the size of that of cementite with six atoms instead of twelve (hence the name Fe_6). The rest of this paper will be dedicated to discussing the properties of the Fe_6 crystal.

The $Pmmn$ crystal was obtained by a naturally symmetry-preserving structural optimization [41]. Its phonon dispersions, reported in Fig. 3(a), still indicate the presence of unstable modes in the vicinity of Γ and Y points in the Brillouin zones. Structural re-optimizations along the pattern of atomic displacements of the unstable zone-center mode produces a new structure with symmetry $Pmn2_1$, shown in Fig. 2(c). This structure is dynamically stable as proved by the absence of imaginary frequencies in its vibrational spectrum (see Fig. 3(b)). To the best of our knowledge this allotrope of iron has not been reported in literature.

The new phase crystal structure is shown in column (c) of Fig. 2. As evident from the top figure, it presents a three-fold modulation on the (001) planes with a asymmetric (two-to-one) “zig-zag” alternation of distorted Fe quadrangles. If one orientation of distorted quadrangles is prevalent on one (001) plane, the opposite occurs on neighbor parallel planes. The resulting ABAB stacking along [001] prevents the formation of mirror planes in the crystal. A comparison with $Pmmn$ Fe_6 (column (b) of Fig. 2) highlights the relationship among the two structures and the deformation induced by the optimization of the $Pmmn$ crystal along its Γ soft mode. The space group of the new optimized structure, $Pmn2_1$, is a subgroup of $Pmmn$. Hereafter, we refer to this new phase as “ $Pmn2_1$ Fe_6 ”. Lattice parameters and atomic positions

$Pmn2_1$ -type Fe_6		
(a, b, c) (Å)	(4.032, 2.464, 7.197)	
Fe_1	(2a)	(0, 0.07044, 0.75564)
Fe_2	(2a)	(0, 0.25046, 0.08932)
Fe_3	(2a)	(0, 0.42873, 0.42311)
$Pmmn$ -type Fe_6		
(a, b, c) (Å)	(7.252, 4.026, 2.460)	
Fe_1	(2b)	(0, 1/2, 0.93204)
Fe_2	(4f)	(0.83069, 0, 0.33549)

TABLE I: Calculated lattice constants and atomic Wyckoff coordinates x, y, z of $Pmn2_1$ and $Pmmn$ Fe_6 at 0 GPa. The (2a), (2b), and (4f) positions are given by $\{(0, y, z), (1/2, -y, z + 1/2)\}$, $\{(0, 1/2, z), (1/2, 0, -z)\}$, and $\{(x, 0, z), (-x, 0, z), (-x + 1/2, 1/2, -z), (x + 1/2, 1/2, -z)\}$, respectively.

for the $Pmmn$ and $Pmn2_1$ Fe_6 crystals are reported and compared in Table I using the Wyckoff notation.

Since the total energy at 0 GPa obtained for this phase is 4.2 mRy/Fe higher than that of the ferromagnetic (FM) bcc crystal, $Pmn2_1$ Fe_6 is a metastable phase of iron. Its M_s (2.47 T) is the highest ever reported for any (meta)stable allotrope of this elemental metal. The unit cell of $Pmn2_1$ Fe_6 can be understood as derived from a $1 \times 3 \times 1$ supercell of a conventional bcc structure (simple cubic lattice with a two-atoms basis) with a slight contraction along [010] ($b/a \sim 2.92$), a substantial elongation along [001] ($c/a \sim 1.65$) and a significant readjustment of ionic positions, producing the above-mentioned structural modulation. Indeed, the appearance of metastable modulated phases along the Bain deformation path from the high-temperature austenite to the low-temperature martensite phases is not uncommon in materials undergoing martensitic transformations. In $Pmn2_1$ Fe_6 , however, the c/a ratio exceeds that of fcc ($c/a = \sqrt{2}$) thus preventing its classification as an intermediate phase between bcc ($c/a = 1$) and fcc. Figure 4 shows volume-preserving deformation energies versus c/a of (a slightly deformed) $Pmn2_1$ Fe_6 (orange line) and of a $1 \times 3 \times 1$ supercell of conventional bcc/bct structure (blue line). The volume, equal to that of the equilibrium structure of $Pmn2_1$ Fe_6 , is 3.8% larger than that of the bcc structure at equilibrium, and 2.3% smaller than that of the fcc crystal optimized with a FM configuration. As seen from the figure, the tetragonal deformation of the bcc cell results in a double-well energy profile in which the bcc structure ($c/a = 1$) represents the global minimum, the fcc ($c/a = \sqrt{2}$) the central maximum, a bct cell with $c/a \sim 1.64$ (compatible with that of $Pmn2_1$ Fe_6) the second (local) minimum. The orange curve in the figure is obtained by changing the value of c/a in an orthorhombic cell with atomic positions compatible to those of the modulated $Pmn2_1$ Fe_6 structure and $b/a = 3$, instead of the equilibrium value 2.92, for a better comparison with the bcc supercell. This curve has only one minimum, in

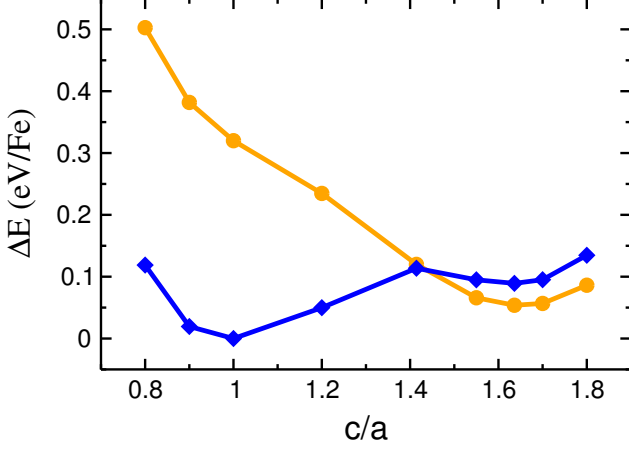


FIG. 4: (Color online) Deformation energy of a $1 \times 3 \times 1$ bcc/bct supercell (blue line) and the $Pmn2_1$ Fe_6 cell (orange line). The deformations are imposed maintaining the volume constant and equal to the equilibrium volume of $Pmn2_1$ Fe_6 .

correspondence of the Fe_6 cell, which is deeper than the local minimum of the distorted bcc supercell energy profile. The two energy curves cross-over in correspondence of the fcc structure, which thus plays the role of a saddle point between the bcc and the $Pmn2_1$ Fe_6 basins, at zero pressure.

Being obtained from a ferromagnetic crystal, $Pmn2_1$ Fe_6 also has a FM ground state. Its AFM and non-magnetic (NM) phases (the latter is actually coincident with fcc, as discussed below) have energies 36 and 75 mRy/atom higher than that of the FM phase, respectively. The magnetic moment and magnetization density of this phase are, respectively, $2.55 \mu_B/\text{Fe}$ and 2.47 T, quite significantly higher than those of the bcc phase ($2.34 \mu_B/\text{Fe}$ or 2.33 T). In fact, to the best of our knowledge, these values are the highest ever reported for any allotrope of Fe. In order to understand the origin of the high magnetization density it is useful to study how this quantity changes with c/a for the two types of distorted cells considered above. Results, shown in Fig. 5, indicate that the bcc supercell has a higher magnetization density than $Pmn2_1$ Fe_6 for all the considered values of c/a , except those in the close vicinity of the Fe_6 stability basin, where the two curves essentially coincide. This observation clarifies that the modulation in the $Pmn2_1$ Fe_6 structure, i.e., the shift of atoms from their bcc equilibrium positions, is only responsible for the stabilization of the Fe_6 orthorhombic crystal but plays a very marginal role in the on-set of its high magnetization. The deviation of b/a from 3 also has negligible effects on M_s . The high magnetization density is, instead, mostly due to the elongation of the c axis that transforms the bcc into a bct cell with $c/a \sim 1.64$. This distortion of the bcc structure changes the order (in energy) of the $3d$ states of iron and

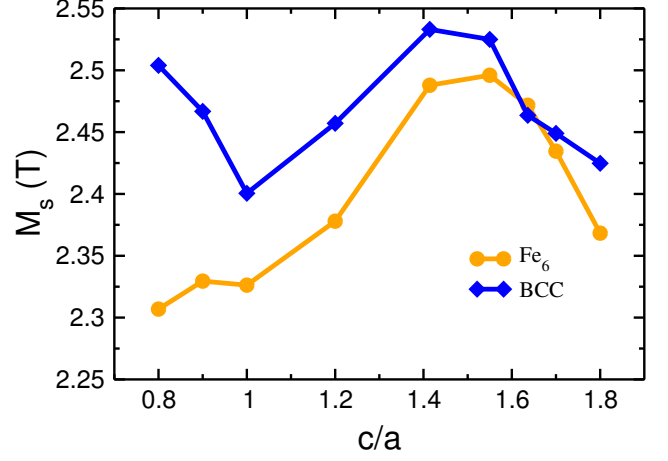


FIG. 5: (Color online) The magnetization density as a function of c/a for a distorted $1 \times 3 \times 1$ bcc supercell (blue line) and for the orthorhombic $Pmn2_1$ Fe_6 (orange line).

allows their occupancies to conform to Hund's rules more closely, thus enhancing magnetization. It is important to note that the FM fcc structure has the highest M_s (~ 2.53 T) among all the phases considered in this study; at the same time, the bcc structure ($c/a = 1$) corresponds to the minimum of M_s along the bcc curve. Because of deviations from their equilibrium volumes, the ground state values of M_s for bcc and FM fcc are different from those reported in Fig. 1 and result in 2.33 T and 2.56 T, respectively.

The magnetic ground state of fcc Fe has been reported to be non-collinear and to consist of a spin spiral incommensurate with the lattice [42, 43]. The spin modulation of the fcc phase represents an intriguing counterpart of the structural modulation that leads to $Pmn2_1$ Fe_6 and stabilizes a FM ground state. To further investigate this aspect, we decided to analyze the vibrational spectrum of the FM fcc crystal. The obtained phonon dispersions indicate the presence of two soft modes along the Σ and Λ lines (see Fig. 6). Soft modes along the Λ line are not very interesting to the present study. In fact, optimizing the unit cell with an ionic displacement pattern corresponding, for example, to the imaginary-frequency mode at $(1/6, 1/6, 1/6)$ merely evolves the fcc structure into the bcc one, along the very well known Bain deformation path. The soft modes along the Σ line are, instead, more interesting. The largest imaginary phonon frequency ($\sim 70i \text{ cm}^{-1}$) occurs at $(\xi, \xi, 0)$ with $\xi \sim 0.4$. To clarify the nature of the structural deformation induced by this soft branch, we studied the soft vibrational mode at $(1/3, 1/3, 0)$, the closest to the minimum of the soft phonon line that is compatible with a supercell of reasonable size ($3 \times 3 \times 1$). By optimizing this supercell of the fcc crystal with atoms moved from their equilibrium positions according to the displacement pattern of

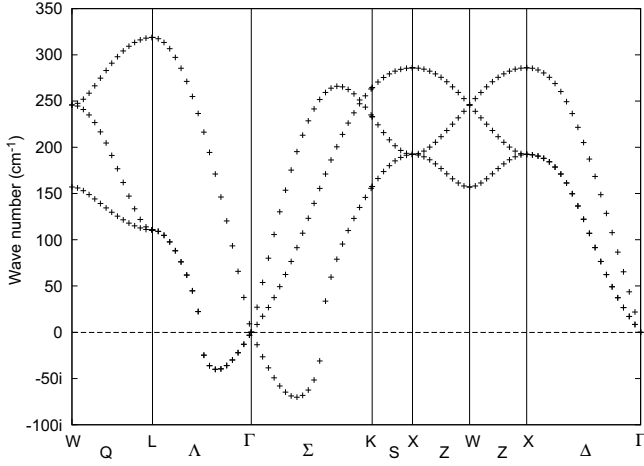


FIG. 6: Phonon dispersion of FM fcc iron at 0 GPa.

this soft mode, a three-fold modulated array of distorted Fe octahedra is obtained. The FM fcc phase transforms into the interim $Pm\bar{m}n$ structure, shown in Fig. 2(b) and, eventually, into $Pmn2_1$ Fe₆, thus highlighting its direct connection with this allotrope. The position of the FM fcc crystal at a saddle point of the energy profile between the bcc and the Fe₆ structures, that emerged from Fig. 4, is thus fully confirmed by the study of its vibrational properties. The presence of a whole band of soft modes along the Σ direction of the Brillouin zone indicates instabilities in the FM FCC crystal at all length scales. The ability to undergo structural distortions, either commensurate, as the one leading to $Pmn2_1$ Fe₆, or incommensurate, could probably be understood as the structural counterpart of the incommensurate magnetic structure (spin-spiral) of the fcc crystal [42, 43]. In short, while a perfectly periodic fcc crystal is characterized by an incommensurate spin-spiral order, a FM ground state can be only stabilized by structural modulations with various periodicities.

It is important to keep in mind that the volume of the FM FCC phase considered above is larger than that of its non magnetic counterpart, and of both bcc and Fe₆ phases. In order to clarify how their relative stability changes with volume and to better understand the relationship between the $Pmn2_1$ Fe₆ crystal and other phases of Fe, it is useful to study the behavior of this allotrope under hydrostatic pressure. Fig. 7 shows the enthalpies of different crystalline structures of Fe (with the FM bcc taken as reference) for pressures between 0 and 50 GPa. At 0 GPa $Pmn2_1$ Fe₆ is more stable than all the other allotropes, and its total energy is 2.9 mRy/atom lower than that of the AFM type-II hcp crystal, a high-pressure form of pristine iron [44] and, up to now, the second most stable phase, after bcc. Finite temperature effects, accounted for by including vibrational terms into the free energy, e.g. within the quasi-harmonic approximation [45], hardly affect the stability. The $Pmn2_1$ Fe₆ remains metastable with respect to the bcc phase at lower pres-

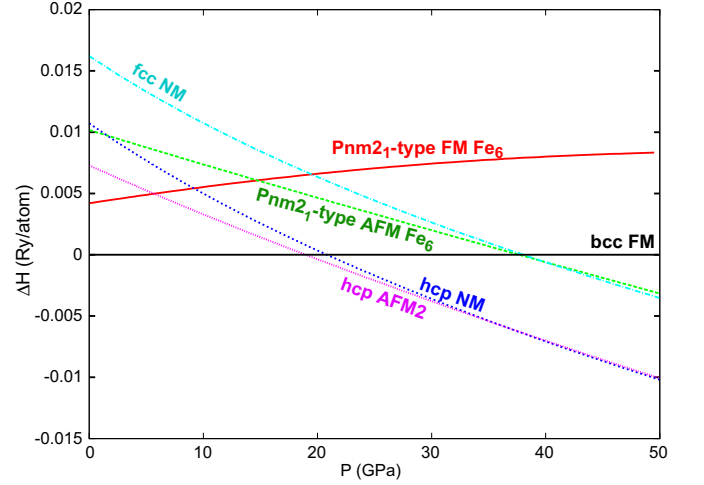


FIG. 7: Relative enthalpies of several iron allotropes with respect to bcc FM iron.

ures. Its free energy at 300 K is 3.9 mRy/atom higher than that of bcc Fe and, even if quantitative details, such as transition pressures, may change with temperature, the overall qualitative picture emerging from Fig. 7 remains unaltered.

Under pressure $Pmn2_1$ Fe₆ undergoes a magnetic transition into an AFM phase (at ~ 15 GPa), followed by a continuous transformation into the NM fcc phase, completed at ~ 40 GPa. Thus we can evince a sort of “magneto-structural duality” between $Pmn2_1$ Fe₆ and fcc Fe: while the FM ground state of the fcc phase can be stabilized by a three-fold modulation compatible with the structure of the $Pmn2_1$ Fe₆, $Pmn2_1$ Fe₆ transforms into fcc under pressure, upon losing its magnetization.

In summary, we found a new metastable allotrope of bulk Fe that is characterized by a unit cell of six atoms with a $Pmn2_1$ space group, and a magnetization density higher than any other known phase. Investigation of this structure highlighted its connection with the bcc and fcc crystals and showed that it can be obtained from a modulation of a $1 \times 3 \times 1$ bcc supercell after imposing an elongation of the c axis up to c/a values of ~ 1.64 . Along the extended Bain deformation path that transforms the bcc structure into the $Pmn2_1$ Fe₆, a collinear-ferromagnetic fcc phase represents an intermediate maximum of the energy (a saddle point) between the bcc and the $Pmn2_1$ Fe₆ phases, and corresponds to the largest bain deformation that does not produce a modulation of atomic positions. This picture is confirmed by the instability of fcc towards both bcc and $Pmn2_1$ Fe₆.

Owing to its high magnetization density, a stabilized Fe₆ could be the starting point to design materials with possibly high magnetic coercivity, for highly technological applications as, for example, lighter-weight electrical engine and power generator rotors, or high information density recording media. In fact, it would be interesting to verify whether a high magnetization-density material can be obtained from $Pmn2_1$ Fe₆ by adding nitro-

gen impurities and, in particular, with a stoichiometry close to that of Fe_{16}N_2 . Unfortunately, the dimension and the complexity of the needed supercell makes this idea quite challenging to test computationally. From the abundant literature on iron and its well consolidated metallurgy, there seems to be little/no evidence that a FM fcc phase can be stabilized at room temperature through addition of doping impurities (except, perhaps, in nanoparticles [46]). However, re-interpreting the structure of α'' Fe_{16}N_2 as a stabilized fcc supercell could provide a key insight to explain its enigmatic giant M_s , and will be the object of future investigations.

I. ACKNOWLEDGMENTS.

Authors are grateful to Prof. R. D. James, Xiaowei Zhang, and Dr. Yanfeng Jiang for very useful discus-

sions. They also thank Daniele Dragoni and Prof. N. Marzari for critically reading the manuscript. The work was supported by the US Department of Energy ARPA-E (Advanced Research Projects Agency-Energy) REACT program under Contract No. 0472-1595. MC acknowledges partial support from the NSF CAREER Award No. DMR 1151738; RMW and MC from the NSF grant No. EAR 1319361. Calculations were performed at the Minnesota Supercomputing Institute and at the Laboratory for Computational Science and Engineering at the University of Minnesota.

-
- [1] F. Ronning and S. Bader (editors). Special section on Rare earth replacement permanent magnets. *J. Phys.: Condens Matter*, 26, 2014.
 - [2] A. Jesche et al. *Nature Communications*, 5:3333, 2014.
 - [3] I. Khan and J. Hong. *Journal of Physics D: Applied Physics*, 47(41):415002, 2014.
 - [4] T. J. Nummy, S. P. Bennett, T. Cardinal, and D. Heiman. *Appl. Phys. Lett.*, 11:99, 2011.
 - [5] B. Balasubramanian, B. Das, R. Skomski, W. Y. Zhang, and D. J. Sellmyer. *Adv. Mater.*
 - [6] S. Yunoki I. S. Elfimov and G. A. Sawatzky. *Phys. Rev. Lett.*, 89:216403, 2002.
 - [7] C. D. Pemmaraju A. Droghetti and S. Sanvito. *Phys. Rev. B*, 78:140404(R), 2008.
 - [8] O. Volnianska and P. Boguslawski. *J. Phys.: Condens. Matter*, 22:073202, 2010.
 - [9] N. E. Christensen H. Emmerich. E. L. Peltzer y Blanca, J. Desimoni and S. Cottenier. *Phys. Status Solidi B*, 246:909 – 928, 2009.
 - [10] V. Lauter L. F. Allard X. Li K. L. Jensen H. Ambaye E. Lara-Curzio N. Ji, M. S. Osofsky and J. P. Wang. *Phys. Rev. B*, 84:245310, 2011.
 - [11] F. Hünigb H. Luekenb W. Kockelmann A. Leinewebera, H. Jacobsa. *J. Alloys and Comp.*, 316:21, 2001.
 - [12] E. Holmström I. A. Abrikosov A. Lindmaa, R. Lizrraga and B. Alling. *Phys. Rev. B*, 88:054414, 2013.
 - [13] W. Xie J. Huang and X. Li. *J. Magn. Magn. Mat.*, 364:1–4, 2014.
 - [14] K. H. Jack. *Proc. R. Soc. London A*, 208:216, 1951.
 - [15] T. K. Kim and M. Takahashi. *Appl. Phys. Lett.*, 20:492, 1972.
 - [16] M. Hanazono M. Komuro, Y. Kozono and Y. Sugita. *J. Appl. Phys.*, 67:5126, 1990.
 - [17] M. Komuro H. Hoshiya Y. Kozono Y. Sugita, K. Mit-suoka and M. Hanazono. *J. Appl. Phys.*, 70:5977, 1991.
 - [18] O. Kitakami S. Okamoto and Y. Shimada. *J. Appl. Phys.*, 79:5250, 1996.
 - [19] J.C. Slater. *J. Appl. Phys.*, 8:385, 1937.
 - [20] L. Pauling. *Phys. Rev.*, 54:899, 1938.
 - [21] R. M. Bozorth. *Phys. Rev.*, 79:887, 1950.
 - [22] G. Dumpich C. Ortiz and A. H. Morrish. *Appl. Phys. Lett.*, 65:2737, 1994.
 - [23] M. Takahashi et al. 76:6642, 1994.
 - [24] M. B. Tian C. Lin D. C. Sun, E. Y. Jiang and X. X. Zhang. *J. Appl. Phys.*, 79:5440, 1996.
 - [25] K. Krishnan M. A. Brewer and C. Ortiz. *J. Appl. Phys.*, 79:5321, 1996.
 - [26] H. Nashi H. Shoji T. Wakiyama M. Takahashi, H. Takahashi and M. Kuwabara. *J. Appl. Phys.*
 - [27] E. Lara-Curzio N. Ji, L. F. Allard and J. P. Wang. *Appl. Phys. Lett.*, 98:092506, 2011.
 - [28] X. Liu-Y. Xu C. Sanchez-Hanke Y. Wu F. M. F. de Groot-L. F. Allard E. Lara-Curzio J. P. Wang, N. Ji. *IEEE Trans. Magn.*, 48:1710, 2012.
 - [29] X. W. Zhang-H. Ambaye J. P. Wang N. Ji, V. Lauter. *Appl. Phys. Lett.*, 102:072411, 2013.
 - [30] S. Ishida and K. Kitawatase. *J. Magn. Magn. Mater.*, 104-107:1933, 1992.
 - [31] B. I. Min. *Phys. Rev. B*, 46:8232, 1992.
 - [32] G. H. O. Daalderop R. Coehoorn and H. J. F. Jansen. *Phys. Rev. B*, 48:3830, 1993.
 - [33] J. M. D. Coey. *J. Appl. Phys.*, 76:6632, 1994.
 - [34] D. S. Sue W. H. Xie and F. S. Li. *J. Phys.: Condens. Matter*, 12:9061, 2000.
 - [35] Z. Nie B. Wang D. Li, Y. Gu and H. Yan. *J. Mater. Sci. Technol.*, 22:833, 2006.
 - [36] M. Richter K. Koepernik E. Şaşıoğlu C. Friedrich H. Sims, W. H. Butler and S. Blügel. 86:174422, 2012.
 - [37] M. van Schilfgaarde T. Kotani L. Ke, K. D. Belashchenko and V. P. Antropov. *Phys. Rev. B*, 88:024404, 2013.
 - [38] X. Liu N. Ji and J.-P. Wang. *New J. Phys.*, 12:063032, 2010.
 - [39] P. Hohenberg and W. Kohn. *Phys. Rev.*, 136:B864, 1964.
 - [40] W. Kohn and L. J. Sham. *Phys. Rev.*, 140:A1133, 1965.
 - [41] R. M. Wentzcovitch. *Phys. Rev. B*, 44:2358, 1991.
 - [42] Y. Nishioka Y. Tsunoda and R. M. Nicklow. *J. Magn. Magn. Mater.*, 128:133, 1993.
 - [43] L. M. Sandratskii M. Uhl and J. Kübler. *Phys. Rev. B*, 50:291, 1994.
 - [44] L. Stixrude G. Steinle-Neumann and R. E. Cohen. *Proc.*

- Nat. Acad. Sci.*, 101:33, 2004.
- [45] D. Wallace. *Thermodynamics of Crystals*. John Wiley, Hoboken, N. J., 1972.
 - [46] R. Pati S. K. Nayak D. J. Singh R. Ma Y. Li Y. Bando S. Nasu B. Wei, M. Shima and P. M. Ajayan. *Small*, 2:804, 2006.
 - [47] P. Giannozzi et al. *J. Phys. Condens. Matter*, 21:395502, 2009.
 - [48] K. Burke J. P. Perdew and M. Ernzerhof. *Phys. Rev. Lett.*, 77:3865, 1996.
 - [49] D. Vanderbilt. *Phys. Rev. B*, 41:R7892, 1990.
 - [50] H. J. Monkhorst and J. D. Pack. *Phys. Rev. B*, 13:5188, 1976.
 - [51] R. M. Wentzcovitch. *Phys. Rev. B*, 44:2358, 1991.
 - [52] J. L. Martins R. M. Wentzcovitch and G. D. Price. *Phys. Rev. Lett.*, 70:3947, 1993.
 - [53] P. Pavone P. Giannozzi, S. de Gironcoli and S. Baroni. *Phys. Rev. B*, 43:7231, 1991.
 - [54] X. Gonze. *Phys. Rev. A*, 52:1086, 1995.
 - [55] A. Dal Corso S. Baroni, S. de Gironcoli and P. Giannozzi. *Rev. Mod. Phys.*, 73:515, 2001.
 - [56] The calculations presented in this article were performed using the plane-wave - pseudopotential codes contained in the Quantum-ESPRESSO package [47]. The

exchange-correlation functional was approximated using a generalized-gradient approximation (GGA), according to the prescription of Perdew-Burke-Ernzerhof (PBE) [48]. The iron pseudopotential was constructed with $3s$ and $3p$ states in the valence manifold and was generated by D. Vanderbilt's method [49] using the $3s^2 3p^6 3d^{6.5} 4s^1 4p^0$ reference electronic configuration. The expansion of electronic wavefunctions and charge density on the plane-wave basis set was converged at kinetic energy cut-offs of 40 and 160 Ry, respectively. A Monkhorst-Pack [50] $8 \times 12 \times 4$ special k-point grid was employed to integrate the Brillouin zone. These parameters guaranteed the convergence of the total energy of the system to within 1 mRy/atom from its limit value. Structural optimizations under finite pressure conditions were performed using the variable-cell-shape damped molecular dynamics technique defined in Refs. [51, 52]. Finite temperature effects were also taken into account using the quasi-harmonic approximation (QHA) [45]. The vibrational spectrum of the material was computed by density-functional-perturbation theory (DFPT) [53–55] as implemented in the PHONON code of the Quantum-ESPRESSO distribution.